UDC 614.3:007.5

Perspective of Creating Low-Cost Medical Assistant Robot Based on Waffle PI4 Platform with Palm Vein Pattern Scanner

Anufriiev V. V., Levchenko O. O., Levchenko Ye. V., Chekubasheva V. A., Glukhov O. V., Galat O. B.

Kharkiv National University of Radio Electronics, Kharkiv, Ukraine

E-mail: *valentyn.anufriiev@nure.ua*

The purpose of this study is to develop a set of modifications for the TurtleBot 3 Waffle Pi robotic platform. One of the key achievements of this work is the creation of a biometric identification system based on the venous pattern of the palm. The principle of operation of the identification system is based on the use of infrared radiation absorbed by hemoglobin in the venous system of the palm. The absorbed radiation creates a clear pattern that can be captured using a camera without an infrared filter. The resulting image is pre-processed to reduce noise and unify with other images for further use in training a convolutional neural network used for patient identification. This identification method allows for high-speed and accurate patient identification, even with dirt or scratches on the palm. The described modifications are aimed at expanding the capabilities of the platform for military medical applications. By integrating these modifications into the TurtleBot 3 Waffle Pi robotic platform, military and civilian hospitals can improve their ability to provide timely and accurate medical care to those in need.

Keywords: robot; TurtleBot; Raspberry Pi; biometrical scanner; image skeletonization; convolutional neural network

Introduction

Military medical facilities and the personnel who serve them play a particularly important role under martial law. Military medicine is currently a fairly developed field in Ukraine that meets all the modern trends typical of developed countries in Europe and the world. Nevertheless, given the overcrowding in hospitals, it is very difficult for staff to provide timely and appropriate assistance to all victims. After analyzing the infectious diseases typical of the military risk group (such as pulmonary tuberculosis, viral hemorrhagic fevers, etc.) [1], it was decided to develop a robotic system, using the best practices of our group's previous studies [2, 3]. It is capable of autonomously performing the typical functions of nursing staff, allowing workers to provide emergency care to soldiers who have suffered serious injuries, such as shrapnel.

1 Related works

A medical assistant robot is an autonomous or semi-autonomous robot designed to assist healthcare professionals in performing various medical tasks, such as surgery, patient care and diagnostics, in a hospital or clinic setting. They are equipped with sensors, cameras, and other technologies to perform tasks with precision and efficiency. In infectious disease wards, robot assistants are of paramount importance due to their ability to minimize the risk of infections. They can perform the following tasks:

- clean and disinfect wards, thereby reducing the workload of healthcare workers and reducing the likelihood of cross-infection [4];

- deliver medicines and supplies, ensuring timely and accurate distribution, while reducing the need for direct contact with patients [5, 6];

- monitor the microclimate in hospital wards, ensuring optimal conditions for patient comfort and recovery, while reducing the risk of infection transmission;

- track the patient's location in the hospital, providing real-time information to medical staff and ensuring timely response to patient needs, thus improving overall patient care and safety [7, 8].

2 Research Methodology

The platform for the modifications is a TurtleBot 3 with a Raspberry Pi 3 as a computing element. This

mobile robot is widely used to maintain sanitary conditions in medical and scientific facilities and as a data collection system. This is all possible due to:

1. open-source software;

2. portability of the design;

3. compatibility with ROS (Robot Operating System);

4. modularity.

In the article, the robot platform paired with the OpenCR module (power supply, spatial orientation) and the Raspberry Pi 3 Model B microcomputer (remote control, control of sensors, disinfection module, and UI-UX interface) [3].

In this work, we propose to replace the Raspberry Pi 3 with the Raspberry Pi 4 as a strategic move designed to yield multiple performance benefits, as substantiated by prior studies. Implemented modifications and schematic diagram of the medical robot assistant are shown in Figure 1. The anticipated advantages encompass heightened processing capabilities and augmented data transfer speed, expedited processing of graphical data, elevated data transfer rates facilitated by the inclusion of a 1Gb Ethernet chip and multichannel Wi-Fi connectivity compliant with 802.11 b/g/n/ac standards, and the prospect of swifter data transmission and an expanded capacity for connected devices, courtesy of BLE 5.0 technology. This proposition enhances the robotic system's operational efficiency and overall capabilities under the proposed research.

OpenCR module using SLAM (simultaneous localization and mapping) for spatial navigation [9–11] remains unchanged. SLAM technique uses a probabilistic approach, which applies a probability distribution to predict the robot's and landmark's location from the generated map. The probability distribution form, P is defined as:

$$P(x_k, m | Z_k, U_k), \qquad (1)$$

where k is time constant, x_k is robot location, Z_k is a sequence of measurements between robot and landmarks assuming one measurement per time step, U_k is a sequence of robot odometry or relative motion.

The process of patient identification involves several steps, the first of which is to obtain an image of the vein pattern of the palm. This is possible because of infrared LEDs and a camera without an IR filter. In this wavelength range (700–900 nm), the absorption coefficient of biological tissues is minimal due to the high water content, which allows you to obtain an image of the palm veins.

Once the image is obtained, useful information is extracted using image preprocessing. For this purpose, standard digital image processing methods were used, including cropping, changing color models, histogram equalization, and skeletonization. Histogram equalization is the process of evenly distributing the intensity of an image to increase contrast.

For each step of image processing, we calculated statistical parameters for analyzing the probability of detecting helpful information, including the signal-to-noise ratio φ, the probability of correct signal detection d, and the probability of false signal detection f.

Signal-to-noise ratio:

$$\varphi = \frac{\mu_s}{\sqrt{\sigma_{S+N}^2}}, \qquad (2)$$

where μ_S is an average value of the signal component of the image, σ_{S+N}^2 is a variance of the signal component with the presence of noise.
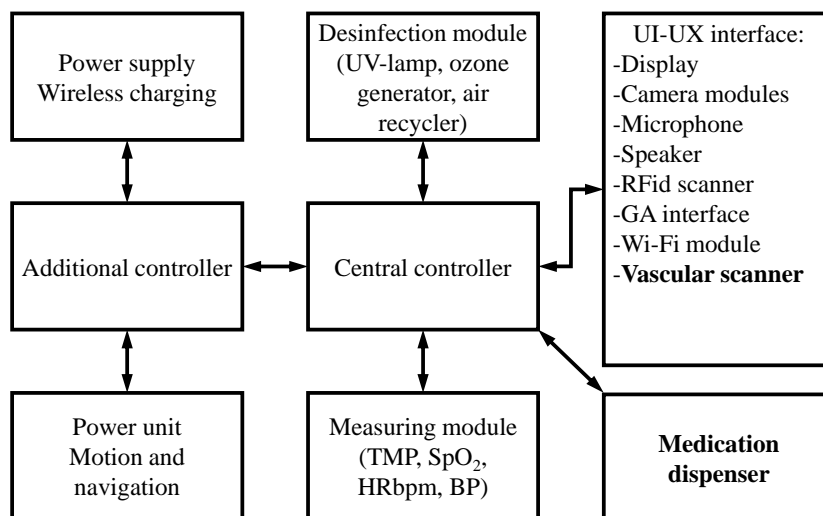

Fig. 1. Block diagram of the medical robot assistant with implemented modifications

Probability of correct signal detection:

$$d = \int_{U_T}^{\infty} \frac{1}{\sqrt{2\pi\sigma_{S+N}^2}} e^{\frac{(U-\mu_{S+N})^2}{2\sigma_{S+N}^2}} \, dU \,, \qquad (3)$$

where μ_{S+N} is an average value of the signal component of the image, U_T is a threshold value.

Probability of false signal detection:

$$f = \int_{U_T}^{\infty} \frac{1}{\sqrt{2\pi\sigma_N^2}} e^{\frac{(U-\mu_N)^2}{2\sigma_N^2}} \, dU \,, \qquad (4)$$

where σ_N^2 is an average value of the signal component of the image, μ_N is an average value of the noise component.

Assuming f as an image represented as a matrix of integer pixel intensities ranging from 0 to $L-1$, where L is the number of possible intensity values, then p denotes the normalized histogram of f with a histogram column for each possible intensity:

$$P_n = \frac{N_n}{\sum_n N} \,, \qquad (5)$$

where N_n is number of pixels with brightnes n, $\sum_n N$ is a total number of pixels.

An image with an aligned histogram g will be determined by the equation:

$$g_{i,j} = \text{floor}\left((L-1)\sum_{n=0}^{f_{i,j}} p_n\right), \qquad (6)$$

where floor() rounds to the nearest lower integer. This is equivalent to converting pixel intensities, k, to f using a function:

$$T(k) = \text{floor}\left((L-1)\sum_{n=0}^{k} p_n\right). \qquad (7)$$

Skeletonization erodes the source image using the specified structuring element that determines the shape of a pixel neighborhood over which the minimum is taken:

$$dst(x,y) = \min_{(x',y')\in\text{element}} src(x+x', y+y'), \qquad (8)$$

where dst is a output image, src is input image.

In this work, we employ a Convolutional Neural Network (CNN) as a robust methodology for identifying and recognizing user's venous patterns. A Convolutional Neural Network is a specialized architecture within the domain of neural networks, extensively employed by the processing and analysis of images and videos [12–15]. Its design is tailored to excel in pattern recognition tasks, showcasing inherited properties that enhance its effectiveness in discerning intricate patterns within visual data. The CNN serves as a powerful tool for the precise identification of venous patterns in the context of current study. A convolutional neural network includes several layers, as shown in Figure 2.

An input layer is used to input information for further processing; Convolutional layer, which applies filters to the input image to create feature maps. These maps highlight specific attributes in the image, such as edges or textures:

$$S(i,j) = \sum_m \sum_n I(i-m, j-n)K(m,n), \qquad (9)$$

where $I(i,j)$ is a pixel value at position (i,j) in the input image, $K(m,n)$ is a filter with size $m \times n$ and $S(i,j)$ is ouput feature map.

After convolution, an activation function is applied, in this case, ReLU, which introduces nonlinearity into the network by zeroing out negative values:

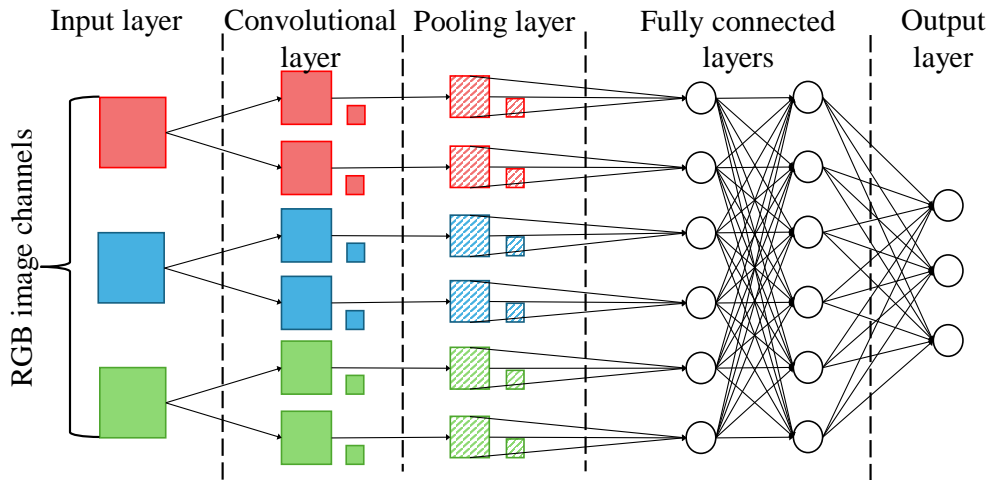$$f(x) = \text{ReLU}(x) = \max(0, x). \qquad (10)$$

Fig. 2. Structure of CNN

The pooling layer is needed to reduce the size of the feature map. In this case, it is MaxPooling, which selects the maximum pixel value in the batch.

$$P(i, j) = \max_{\forall(x,y)\in\text{Pool}(i,j)} S(m, n). \qquad (11)$$

After the pooling layer, the output data passes to the fully connected layer, which integrates the high-level features extracted by the previous layers to perform the final task, namely, classifying the input image:

$$y = f\left(\sum_i w_i x_i + b\right), \qquad (12)$$

where w_i is a weights, x_i is a input values, b is a bias and f is an activation function.

After the fully connected layer, the data is transferred to the output layer, which is used to produce the final result.

3 Results

A palm vein pattern scanner is used to provide contactless identification. This type of biometric identification was chosen due to its high level of identification accuracy, high resistance to changes over time and injuries to the palm veins, and the absence of the need for physical contact with the scanner.

The identification system consists of a computing module, a camera without an IR filter, and an IR LED unit. The computing module is a central robot controller (Raspberry Pi 4), and the camera is a Raspberry Pi Camera module 3 NoIR. The block diagram of the device is shown in Figure 3.
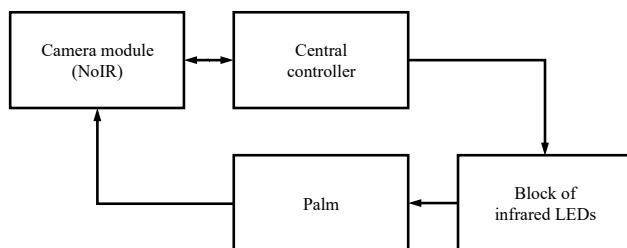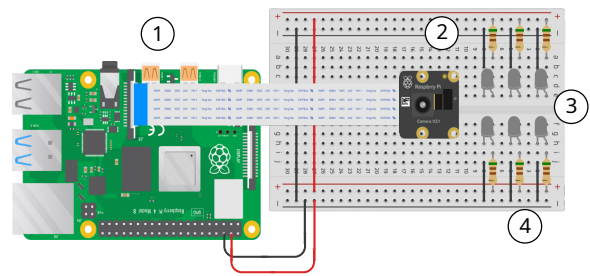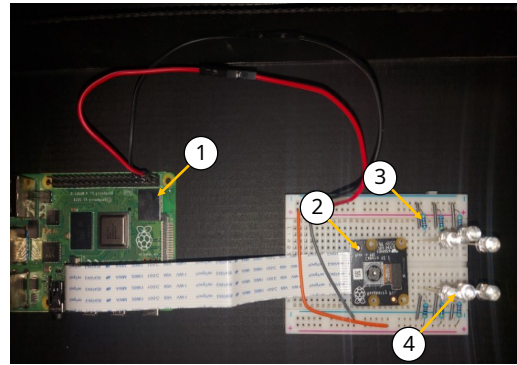
Fig. 3. Block diagram of the palm vein pattern scanner

The implemented device consists of: Raspberry Pi 4B (1), Raspberry Pi Camera module 3 NoIR (2), IR LEDs (3), resistors (4) and is shown in Figure 4.

(a)

(b)

Fig. 4. Schematic of palm vein scanner (a), experimental setup (b)

Notably, the Raspberry Pi 4b empowers the robot to gather and transmit data across longer distances at elevated speed, all while reducing overall energy consumption.

Algorithm of the device operation [16] is shown on Figure 5, and goes by following steps:

1. camera initialization and power supply to the LEDs;

2. take a picture of the palm;

3. image processing;

4. patient identification.

To perform image processing, we implemented the code using the Python programming language, leveraging the capabilities of the OpenCV and NumPy libraries.

The sequence of image processing steps is illustrated in Figure 6, delineating the various stages involved in the computational manipulation of the image data and described below:

1. image resizing and converting to grayscale. These operations reduce information about the color parameters of the image, simplifying the data for further processing. This initial panel represents the raw, unprocessed image with minimal contrast between the venous structure and the background. Here, details are limited, and the target patterns are poorly distinguished from surrounding noise;

2. noise reduction by smoothing the histogram. This step significantly reduces random pixel intensity variations, smoothing out the image and clarifying major structures while removing extraneous noise that could obscure finer details;

3. converting the image to the YUV color model, and histogram equalization is applied to the Y channel (brightness). This step improves brightness and contrast while preserving the color information in the U and V channels. By selectively amplifying the target features, this step increases the overall contrast of the venous pattern, helping distinguish it from the background with greater clarity;

4. skeletonization reduces the image to its basic structure, preserving only key shapes. This process reduces the venous structure to its essential contours, creating a 'skeleton' of the pattern. As a result, only the primary lines of the venous network are retained, offering a clear and highly contrasted representation of the vascular structure without background interference. This stage is especially useful for precise identification of structural boundaries, as it isolates the most significant linear features of the pattern.

Based on the obtained results we also plotted the probability density of the signal and noise components that are demonstrated in Fig. 7.
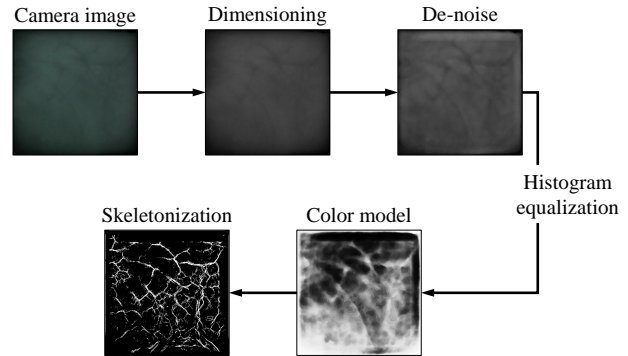

Fig. 6. Stages of image analyzing and processing

Fig. 7a shows that the pixel brightness distribution shows a clear signal with a distinct peak, which means that the grayscale image can still be recognized against the background of the noise component, but the probability of false pattern recognizing is high. Histogram equalization improved the detection probability (Fig. 7b), although it did not solve the problem of false positives. Changing the color model to YUV distributes the signal at higher brightness levels. This step allows to expand the range of signal brightness over the entire spectrum (Fig. 7c). Skeletonization changed the content of the image, resulting in a predominantly black background and areas of increased brightness for the signal component representing the venous pattern. This is reflected by a high concentration of background components only at lower brightness levels, while the signal is present over a wide brightness range. At the same time, the probability of correct detection of the signal increases due to the fact that the intersection of the histograms of the useful signal and the background is minimized (Fig. 7d). The results are presented in Table 1.
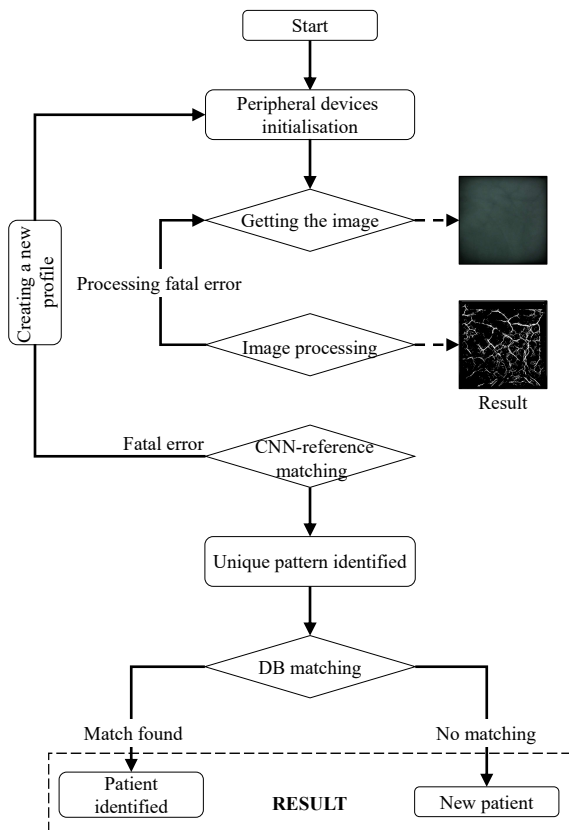
Figure 8 presents a comparative plot illustrating pixel intensity distribution across a defined line segment in the image, demonstrating how each stage of processing affects the contrast and clarity of the venous pattern. The plot shows four distinct lines, each corresponding to one stage of image processing: the dimensioned image (*orange line*), the de-noised image (*blue line*), the color-adjusted image (*green line*), and the skeletonized image (*red line*). This comparative analysis allows for a quantitative assessment of the effects of each processing step on the intensity distribution.
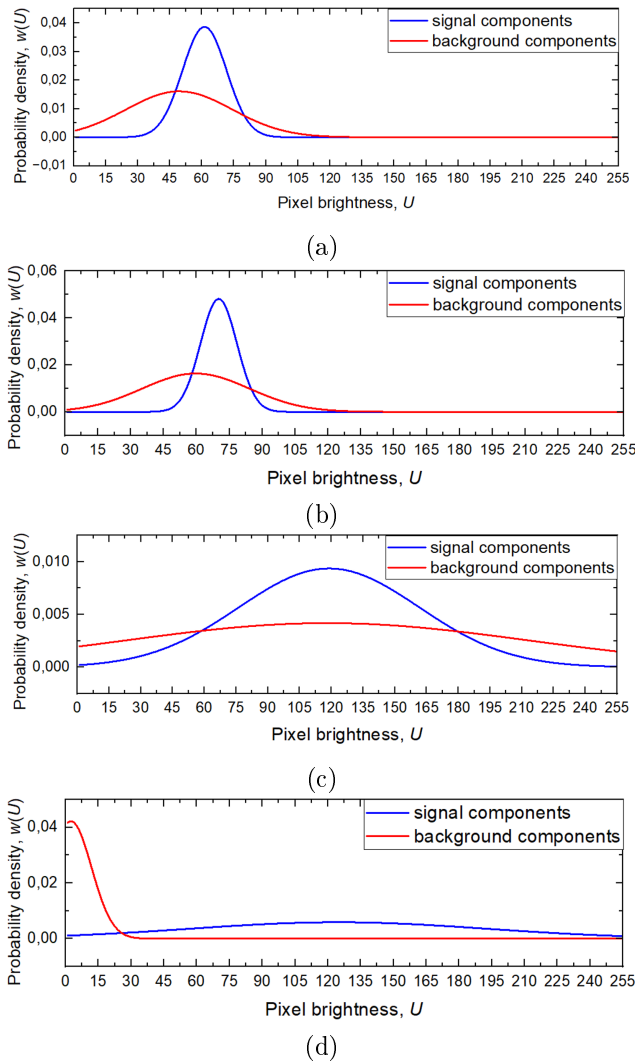

Fig. 5. Algorithm of the device operation

(a)

(b)

(c)

(d)

Fig. 7. Probability density of the signal and noise components of image processing stages for (a) dimensionig image with changed color scheme to gray shades process, (b) histogram equalization process, (c) convertation to YUV color model process, (d) image skeletonization process

Initially, the *orange line* representing the unprocessed image shows significant fluctuations, also indicating a high level of noise and limited contrast between the venous structure and the background. This variability in pixel intensity suggests that fine details of the venous pattern are masked by random noise and low contrast, making it difficult to identify distinct vascular features. Following de-noising (*blue line*), the intensity fluctuations decrease, demonstrating successful noise reduction. Current step smooths the intensity profile, reducing extraneous variations and beginning to reveal the underlying structure more clearly.

With the change in color model (*green line*), the venous pattern becomes even more pronounced, as indicated by sharper peaks and valleys in the intensity plot. This adjustment enhances the contrast, particularly highlighting the venous structure against the background tissue. The final *red line*, representing the skeletonized image, shows the most distinct intensity peaks, corresponding to the core lines of the venous structure, while the background intensity remains minimal. This stage isolates the primary edges of the venous network, providing a high-contrast and simplified representation of the pattern, which is essential for precise structural analysis.

The calculated parameters according to formulas (2), (3), (4) is presented in Table 1 and illustrated how each image processing stage progressively enhances signal clarity and reduces noise interference, ultimately improving the detectability of the venous pattern.

Initially, the parameter φ, which indicates the average signal-to-noise ratio, increases from the initial dimensioning stage to reach its highest value after skeletonization. This rise in φ demonstrates that each processing step strengthens the contrast between the venous pattern and the background, with skeletonization providing the clearest delineation.
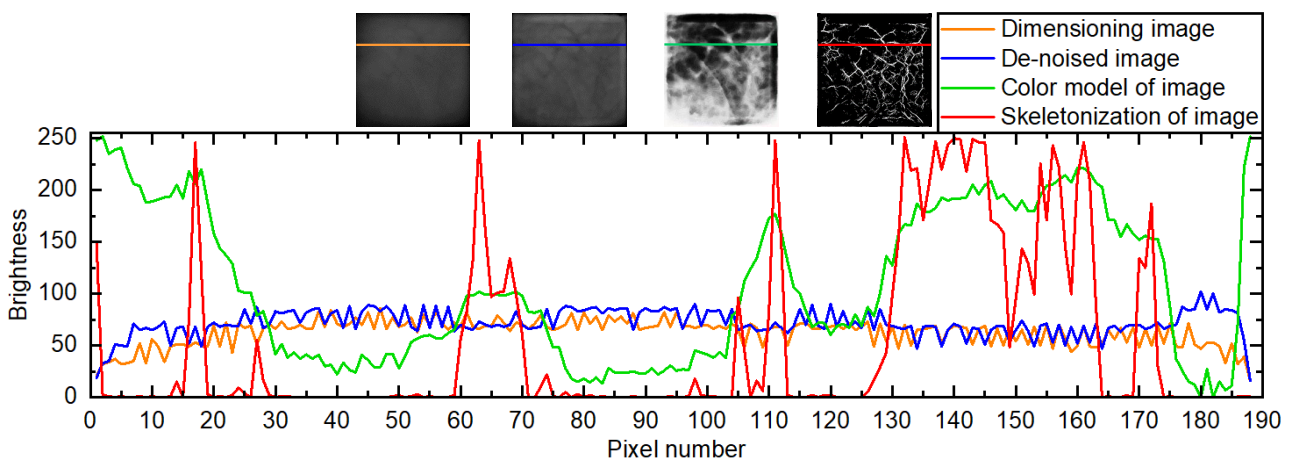

Fig. 8. Stages of image analyzing and processing

Табл. 1 Results of calculating statistical parameters

Step	φ	d	f
Dimensioning	1,149	1	0,975
De-noise	1,262	1	0,992
Change of color model	0,022	0,997	0,816
Skeletonization	1,809	0,940	0,580

Similarly, the signal-to-noise ratio d remains stable through de-noising but declines slightly by the final stage, likely reflecting the reduction of extraneous intensity variations as the image focuses on core structural features. The probability of false signal detection f, decreases progressively with each processing step, particularly after color model adjustment and skeletonization, indicating a significant reduction in noise-related artifacts that could otherwise be misidentified as features. Together, these results affirm that each stage of image processing incrementally improves the distinctness of the venous pattern and minimizes the likelihood of noise-induced errors, thus enhancing the overall accuracy and reliability of the image analysis.

The structure of the neural network was undertaken using the Python programming language as well as for the imaging processing and shown on Figure 9, where we utilized the TensorFlow Keras library – an open-source machine learning software framework. This framework provides a comprehensive suite of tools and functionalities for the development, training, and evaluation of neural networks, ensuring a robust and efficient implementation of given model.
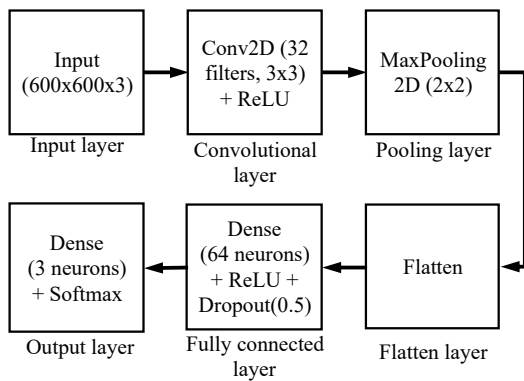
Fig. 9. Structure of developed CNN

Finally, the performance of the neural network was evaluated by evaluating accuracy (Fig. 10a) and training losses (Fig. 10b). As can be seen from the graphs, after the fifth training epoch, the accuracy and loss stop changing, this is due to the fact that the shading dataset is quite small and the network has reached its peak accuracy and loss. But in general, the graphs show a significant increase in accuracy, in particular, the constructed convolutional neural network is characterized by a recognition accuracy of 83.3%.
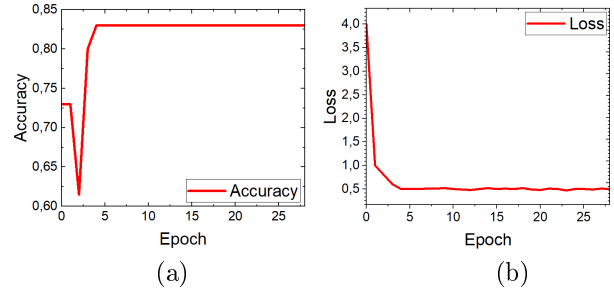
Fig. 10. Plot of accuracy with each training epoch (a) and schedule of losses during training (b)

4   Disscusion

This article presents a number of modifications aimed at turning it into a robot assistant for medical institutions. The prototype of the palm vein pattern scanner demonstrates its performance in laboratory conditions, but there are ways to develop it, including:

- changing the design of the scanner, which includes changing the location of the IR LEDs to increase the contrast of veins against the palm and compensate for the effects of palms with different thicknesses [17];

- installing a polarising filter between the camera and the LEDs, this will increase the colour saturation and reduce the amount of reflected radiation (increasing the colour saturation of the scene and suppressing unwanted reflections) [14];

- increasing the size of the dataset for training the neural network, which will make it possible to identify the patient with greater accuracy [18,19].

Conclusions

The scope of this study has revealed the potential for the adaptation and enhancement of a cost-effective medical robot-assistant, poised for both military and civilian applications. The core innovation underpinning this progress revolves around replacing the Raspberry Pi 3b microcomputer with its more advanced counterpart, the Raspberry Pi 4b. This transition has ushered in significant advancements, particularly in computational efficiency. One of the most notable improvements from this microcomputer upgrade is the remarkable acceleration in the robot's computational capabilities. By harnessing the enhanced processing power of the Raspberry Pi 4b, obtained device can perform calculations with noteworthy celerity, contributing to quicker decision-making and more responsive interactions.

A biometric patient identification system based on the palm venous pattern was implemented, which includes a Raspberry Pi and an infrared camera on

the hardware side and a convolutional neural network on the software side. Using standard image processing techniques combined with a convolutional neural network allowed us to obtain patient identification accuracy (83.3%), which is satisfactory for datasets with a small training sample. Another feature of the system is its modularity, which increases the system's maintainability, as in the event of a malfunction or need for replacement, the Raspberry Pi can be easily dismantled and replaced with a new device without the need to reconfigure other system components. This flexibility in the use and maintenance of the system allows for efficient maintenance.

In addition to the above, another advantage of using the TurtleBot Waffle Pi mobile platform is its modular structure. This feature allows easy installation of new modifications and their removal in case of breakdown.

Together, these innovations represent a significant improvement over the previously developed autonomous system. The results of this work have the potential not only to provide assistance in the field of medical care, but can also be implemented in the military field as an effective assistant robot technology for monitoring the condition of wounded soldiers.

References

[1] Liu, G.-D. et al. (2021). Military medical research on internal diseases in modern warfare: new concepts, demands, challenges, and opportunities. *Military medical research*, Vol. 8, Article number: 20. DOI:10.1186/s40779-021-00313-8.

[2] Chekubasheva, V. et al. (2022). Possibility of Creating a Low-Cost Robot Assistant for Use in General Medical Institutions During the COVID-19 Pandemic. In: Blaschke, D., Firsov, D., Papoyan, A., Sarkisyan, H.A. (eds) Optics and Its Applications. *Springer Proceedings in Physics*, Vol 281, pp. 203–213. DOI:10.1007/978-3-031-11287-4_16.

[3] Chekubasheva, V. A. et al. (2022). Creating of a remote-presence robot based on the development board Texas Instruments to monitor the status of infected patients. *Biosensors and bioelectronics: X*, Vol. 11, 100215. DOI:10.1016/j.biosx.2022.100215.

[4] Yao, Z., Ma, N. and Chen, Y. (2023). An Autonomous Mobile Combination Disinfection System. *Sensors*, Vol. 24 (1), 53. DOI:10.3390/s24010053.

[5] Chelvam, Y. K., Zamin, N. and Steele, G. S. (2014). A Preliminary Investigation of M3DITRACK3R: A Medicine Dispensing Mobile Robot for Senior Citizens. *Procedia computer science*, Vol. 42, pp. 240–246. DOI:10.1016/j.procs.2014.11.058.

[6] Fauzi, R., Mustari, A. та Lutfiyana. (2023). Medical Assistant Robot With Patient Trajectory Reading Based on Odometry using Photovoltaic source. *IOP Conference Series: Earth and Environmental Science*, 1157, 012043. DOI:10.1088/1755-1315/1157/1/012043.

[7] Vasco, V. et al. (2022). HR1 Robot: An Assistant for Healthcare Applications. *Frontiers in Robotics and AI*, Vol. 9, 813843. DOI:10.3389/frobt.2022.813843.

[8] Bathirappan, K. et al. (2022). Patient monitoring and medicine dispenser robot. *AIP Conf. Proc.*, Vol. 2494, Iss. 1, 030004. DOI:10.1063/5.0106604.

[9] Choi, K.-S. and Lee, S.-G. (2010). Enhanced SLAM for a mobile robot using extended Kalman Filter and neural networks. *International journal of precision engineering and manufacturing*, Vol. 11, Iss. 2, pp. 255–264. DOI:10.1007/s12541-010-0029-9.

[10] Xu, Y. et al. (2021). Distributed Kalman filter for UWB/INS integrated pedestrian localization under colored measurement noise. *Satellite navigation*, Vol. 2, Article number: 22. DOI:10.1186/s43020-021-00053-z.

[11] Beresnev, V. et al. (2021). Creation of a Prototype of a Multi-function Remote Presence Robot for Physical Research in Electronics. *Journal of Nano- and Electronic Physics*, Vol. 13, Num. 5, p. 05039-1. DOI:10.21272/jnep.13(5).05039.

[12] Yang, S. et al. (2021). Intelligent Health Care: Applications of Deep Learning in Computational Medicine. *Frontiers in Genetics*, Vol. 12:607471. DOI:10.3389/fgene.2021.607471.

[13] Knok, Ž., Pap, K. and Hrnčić, M. (2019). Implementation of intelligent model for pneumonia detection. *Tehnički glasnik*, Vol. 13, Iss. 4, pp. 315–322. DOI:10.31803/tg-20191023102807.

[14] Stanuch, M., Wodzinski, M. and Skalski, A. (2020). Contact-Free Multispectral Identity Verification System Using Palm Veins and Deep Neural Network. *Sensors*, Vol. 20, Iss. 19, 5695. DOI:10.3390/s20195695.

[15] Alzubaidi, L. et al. (2021). Review of deep learning: concepts, CNN architectures, challenges, applications, future directions. *Journal of Big Data*, Vol. 8, Article number: 53. DOI:10.1186/s40537-021-00444-8.

[16] Wu, W. et al. (2020). Review of palm vein recognition. *IET Biometrics*, Vol. 9(1), pp. 1–10. DOI:10.1049/iet-bmt.2019.0034.

[17] Crisan, S. et al. (2007). Vein pattern recognition. Image enhancement and feature extraction algorithms. *IMEKO*, 5 p.

[18] Althnian, A. et al. (2021). Impact of Dataset Size on Classification Performance: An Empirical Evaluation in the Medical Domain. *Applied sciences*, Vol. 11, Iss. 2, 796. DOI: 10.3390/app11020796.

[19] Hirahara, D. et al. (2020). Effects of data count and image scaling on Deep Learning training. *PeerJ. Computer science*, 6(e312), p. e312. DOI: 10.7717/peerj-cs.312.

Перспектива створення бюджетного робота-асистента для медичних закладів на базі платформи Waffle PI4 зі сканером венозного рисунка долоні

Ануфрієв В. В., Левченко О. О., Левченко Є. В., Чекубашева В. А., Глухов О. В., Галат О. Б.

Розроблено комплекс модифікацій для роботизованої платформи TurtleBot 3 Waffle Pi. Одним із ключових досягнень даної роботи є створення системи біометричної ідентифікації на основі венозного рисунка долоні. Робота системи ідентифікації заснована на використанні інфрачервоного випромінювання, що поглинається гемоглобіном венозної системи долоні. Поглинуте випромінювання створює чіткий візерунок, який можна зафіксувати за допомогою камери без інфрачервоного фільтра. Отримане зображення попередньо обробляється для зменшення шуму та уніфікації з іншими зображеннями для подальшого їх використання у тренуванні згорткової нейронної мережі, що використовується для ідентифікації пацієнта. Даний метод ідентифікації дозволяє з високою швидкістю і точністю ідентифікувати пацієнта, навіть при наявності бруду або подряпин на долоні. Описані модифікації спрямовані на розширення можливостей платформи для військово-медичного застосування. Інтегруючи ці модифікації в роботизовану платформу TurtleBot 3 Waffle Pi, військові та цивільні госпіталі можуть покращити свої можливості з надання своєчасної та точної медичної допомоги тим, хто її потребує.

Ключові слова: робот; TurtleBot; Raspberry Pi; біометричний сканер; скелетонізація зображення; згорткова нейронна мережа